scientific reports

OPEN

Effect of nanoparticulate CaCO$_3$ on the biological properties of calcium silicate cement

Quang Canh Vo[1,2], Gitae Son[1,2], Gyeung Mi Seon[1], Sun Woo Um[1], Sang Hoon Choi[1] & Hyeong-Cheol Yang[1✉]

This study aimed to evaluate the effects of nanoparticulate CaCO$_3$ (NPCC) on the biological properties of calcium silicate-based cements (CSCs), including their cytotoxicity, in vitro osteogenic activity, and interactions with rat femur tissue. The average size of NPCC was 90.3±26.0 nm. Cytotoxicity and osteogenic activity assays were performed using mouse bone marrow mesenchymal stem cells (BMSCs). BMSCs exposed to the eluents from CSC alone and CSC containing 2.5% NPCC (CSC-NPCC (2.5%)) for 24 h showed decreased cell viability at an eluent concentration of 75%. In contrast, CSC-NPCCs (5%, 10%, and 20%) did not affect cell viability. Regarding osteogenic activity, CSC-NPCCs (5%, 10%, 20%) enhanced the expression of osteogenic genes, including runt-related transcription factor 2 (RUNX2), alkaline phosphatase (ALP), type I collagen (COL-1), and osteocalcin (OCN). Additionally, mineralization in cell cultures was enhanced by CSC-NPCC, indicating that NPCC promoted the osteogenic activity of CSCs. In rat femurs, NPCC accelerates CSC resorption and stimulates bone regeneration at the implantation site. CSC alone occupied 22.2%±3.25% of the total femoral area at the implantation site, whereas CSC-NPCC (20%) occupied only 4%. These histological findings suggest that CSC-NPCC has potential as a biodegradable bone cement for use in bone defect areas that require regeneration.

Keywords Nanoparticulate calcium carbonate, Calcium silicate cement, Bone marrow mesenchymal stem cells, Biocompatibility, Osteogenic, Bone regeneration

Calcium silicate-based cements (CSCs), such as mineral trioxide aggregates (MTA), are used in various endodontic dental treatments, including pulp capping, apexification, and root-end filling[1–3]. MTA is a mixture of refined Portland cement and bismuth oxide, a radiopaque agent. Portland cement, which is primarily composed of tricalcium silicate and dicalcium silicate, produces calcium silicate hydrate and calcium hydroxide upon hydration in water. The ability of MTA to set well under high-moisture conditions makes it an ideal material for use in wet environments, such as the oral cavity[4]. Furthermore, MTA exhibits antimicrobial activity and excellent biocompatibility, stimulating the formation of hard tissues[5,6]. When directly applied to the dental pulp, MTA can initiate dentinogenesis, followed by the formation of a dentin bridge, which helps protect the underlying pulp tissues and maintain vitality. The osteogenic activity of MTA has also been demonstrated in vitro using osteoblasts and mesenchymal stem cells[7,8]. These findings indicate the utility of MTA in the repair of tooth roots, where optimal sealing properties and bone-forming activity are critical.

Previous reports have shown that MTA sets slowly within approximately 3 h[9]. The relatively prolonged setting time of MTA is a significant limitation for its clinical application, as it increases the risk of the material being washed out before it has completely set. To address the drawback of MTA, various additives have been tested as setting accelerators[10,11]. The addition of calcium chloride to MTA was shown to significantly reduce the setting time[12], and calcium carbonate (CaCO$_3$) accelerated the hydration of Portland cement, resulting in a decreased setting time[13,14]. The beneficial impact of CaCO$_3$ on MTA hydration was also demonstrated. The addition of nanoparticulate calcium carbonate (NPCC) accelerated the setting time and reduced the dimensional changes in MTA[15]. Therefore, CaCO$_3$ has the potential to enhance the clinical utility of CSCs. Certain commercial CSC products incorporate calcium carbonate, which has a short setting time[16,17].

CSC products vary in their components, and these variations influence their biological properties, such as cytotoxicity and osteogenic activity[18,19]. CaCO$_3$ may also potentially influence the bioactivity of CSC, in addition

[1]Department of Dental Biomaterials Science, Dental Research Institute, School of Dentistry, Seoul National University, 101 Daehak-ro, Jongno-gu, Seoul 03080, South Korea. [2]Quang Canh Vo and Gitae Son contributed equally. ✉email: yanghc@snu.ac.kr
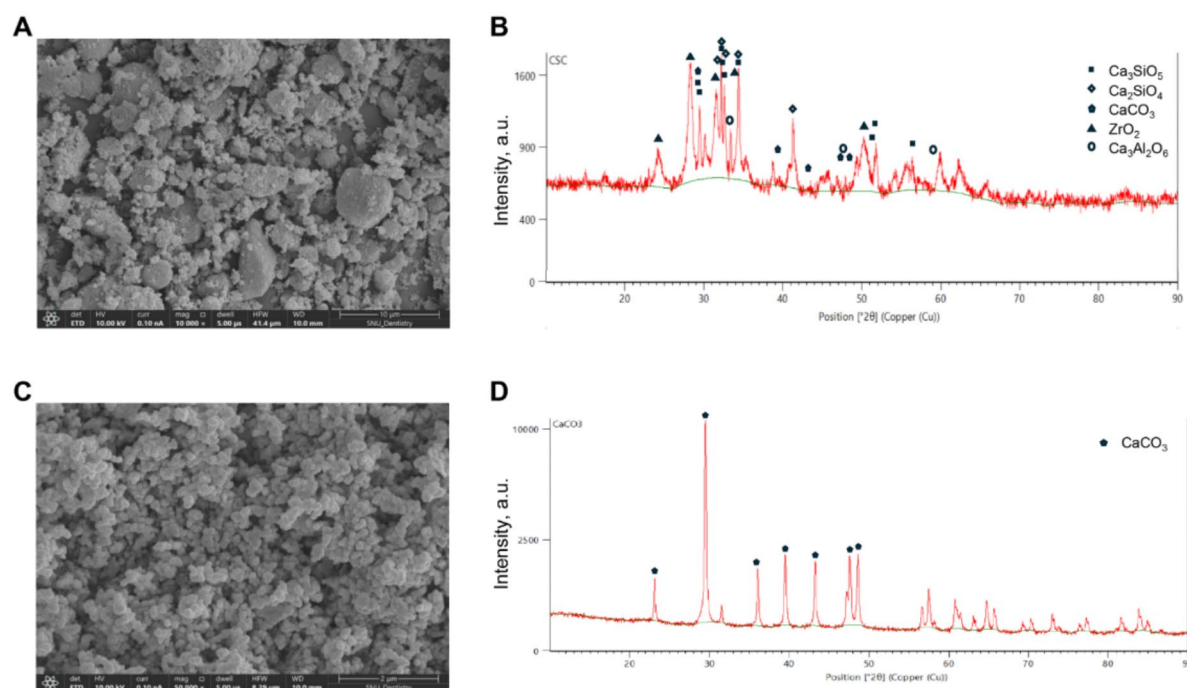
Fig. 1. Morphology and XRD patterns of CSC powder and NPCC.

	0% NPCC	**2.5% NPCC**	**5% NPCC**	**10% NPCC**	**20% NPCC**
Setting time (min)	55.78 ± 1.21^a	45.28 ± 0.92^b	44.43 ± 0.83^b	38.10 ± 0.96^c	37.81 ± 0.94^c
Compressive strength (MPa)	14.3 ± 0.54^a	16.93 ± 1.59^b	16.83 ± 1^b	14.39 ± 0.71^a	11.18 ± 0.58^c
Solubility (%)	2.39 ± 0.34^a	1.16 ± 0.15^b	$1.82 \pm 0.44^{a, b}$	1.29 ± 0.15^b	1.36 ± 0.33^b
Dimensional change (%)	0.468 ± 0.174^a	0.643 ± 0.107^a	0.396 ± 0.106^a	0.462 ± 0.048^a	0.484 ± 0.084^a

Table 1. Physicomechanical properties of CSC-NPCC. Data are presented as mean±standard deviation (n=5). Different superscript letters in the same row represent statistically significant differences among the groups ($P < 0.05$), and the same letters indicate no significant difference ($P > 0.05$).

to its physical properties, such as setting time. In this study, to investigate the effects of $CaCO_3$ on the biological activities of CSC, we mixed CSC with $CaCO_3$ at varying ratios and evaluated the cytotoxicity, in vitro osteogenic activity, and interaction with rat femur tissue.

Results
SEM morphology and chemical composition of CSC and NPCC
Figure 1A and B show the scanning electron microscopy (SEM) images and X-ray diffraction (XRD) patterns of the CSC powder synthesized in this study. The peaks in the XRD pattern indicate the presence of tricalcium silicate (C3S) ($2\theta = 29.3°$, $32.1°$, $32.5°$, $34.3°$), dicalcium silicate (C2S) ($2\theta = 32.1°$, $32.6°$, $34.3°$, $41.2°$), tricalcium aluminate (C3A) ($2\theta = 33.2°$, $47.6°$, $59.2°$), and zirconium dioxide (ZrO_2) ($2\theta = 28.2°$, $31.5°$, $34.2°$, $50.1°$). This demonstrates that the main component of the synthesized powder was CSC. The morphology of NPCC is shown in Fig. 1C. The average particle size in the SEM image was 90.3 ± 26.0 nm (diameter). The peak XRD pattern of NPCC matched that of calcite (Fig. 1D).

Effects of NPCC on physicomechanical properties of CSC
The mechanical and physical properties of CSC-NPCC are listed in Table 1. CSC without NPCC exhibited 55.78 ± 1.21 min of setting time. The setting time of the CSC decreased as the concentration of NPCC increased.

CSC-NPCC (20%) showed the lowest setting time, 37.81 ± 0.94 min. However, there was no statistical difference in the setting time between CSC-NPCC (10%) and CSC-NPCC (20%), indicating that the reducing effect of NPCC on the setting time of CSC was limited at the NPCC concentration above 10%. The compressive strength of CSC was also affected by NPCC. 2.5% NPCC induced the highest compressive strength, followed by a decrease in compressive strength with increasing NPCC concentration. The solubility was generally lowered by the addition of NPCC, but not in a concentration-dependent manner. At 5% NPCC, there was no statistically significant difference in solubility from CSC without NPCC. Finally, the dimensional changes in CSC in distilled water (DW) were not significantly affected by NPCC at all the concentrations.

Data are presented as mean ± standard deviation ($n=5$). Different superscript letters in the same row represent statistically significant differences among the groups ($P<0.05$), and the same letters indicate no significant difference ($P>0.05$).

Cytotoxicity and osteogenic activity of CSC-NPCC

The cytotoxicity of the CSC-NPCC eluents was evaluated after 24-h and 7-d treatments. When bone marrow mesenchymal stem cells (BMSCs) were treated for 24 h, the cell viability was significantly decreased by 75% eluents of CSC-2.5% NPCC and CSC alone (Fig. 2A). The other groups of CSCs containing higher amounts of NPCC did not show reduced cell viability at 75% eluent. These findings indicated that NPCC reduced the cytotoxic effects of CSC at elevated concentrations, specifically 5%, 10%, and 20%. The cell treatment for 7 d caused a significant decrease in cell viability at 75% eluent in all groups of cements, among which CSC-NPCC (2.5%) showed the lowest cell viability, 7.2% ± 1%, followed by CSC-NPCC (0%). The 50% eluent decreased cell viability in the groups of CSC-NPCC (0%, 2.5%, 20%), but not in CSC-NPCC (5% and 10%). CSC-NPCC (10%) exhibited the highest cell viability in both 50% and 75% eluents (Fig. 2B).

The effect of CSC-NPCC on the osteogenic differentiation of BMSCs was evaluated using 25% of the eluent, the highest nontoxic concentration of the eluent. The expression levels of runt-related transcription factor 2 (RUNX2), alkaline phosphatase (ALP), type I collagen (COL-1), and osteocalcin (OCN) were not significantly affected by CSC alone or by CSC-NPCC (2.5%). In contrast, CSC-NPCC (5%, 10%, and 20%) enhanced the expression of these marker genes, with the exception of COL-1, which remained unaltered by CSC-NPCC (10%) (Fig. 3). The extent of mineralization observed in the cement-treated cells was positively correlated with the mRNA expression levels of the osteogenic marker genes. CSC-NPCC (5%, 10%, and 20%) significantly increased the mineralization of BMSC cultures (Fig. 4). These results indicated that the incorporation of NPCC into CSC enhanced the osteogenic differentiation of BMSCs at concentrations greater than 5%.

Tissue responses to CSC-NPCC in rat femur

Unset CSC-NPCC was implanted into rat femurs to evaluate the cement resorption and bone regeneration in the implanted area. Histological analysis using hematoxylin and eosin (H&E) staining was conducted on the
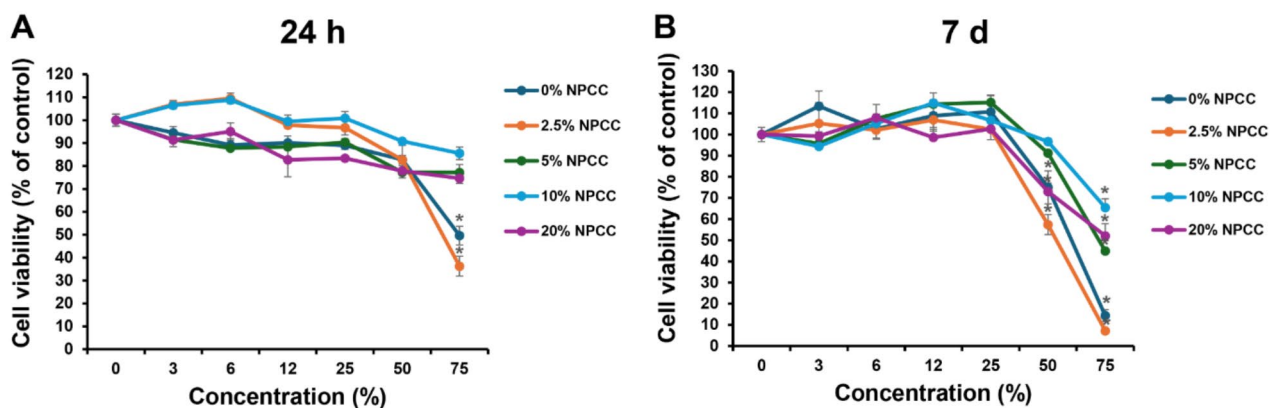
Fig. 2. Cell viability of BMSCs treated with eluent dilutions of CSC-NPCC for 24 h and 7 d. *$P<0.05$ compared with the control value. Three replicate experiments were performed ($n=3$).
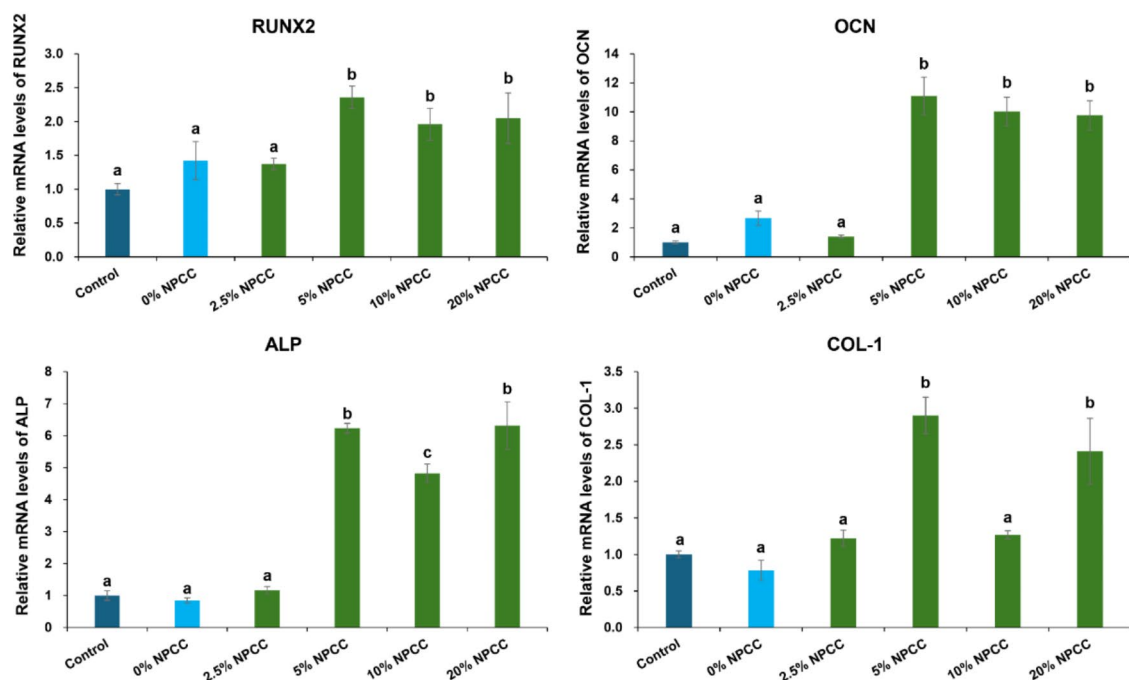
Fig. 3. Relative mRNA expression of osteogenic markers in BMSCs after 10 d of culture in CSC-NPCC eluents. Data are presented as mean ± standard deviation from three independent experiments ($n = 3$). Data bars labeled with different letters indicate statistically significant differences among the groups ($P < 0.05$), whereas bars with the same letters indicate no significant difference ($P > 0.05$).
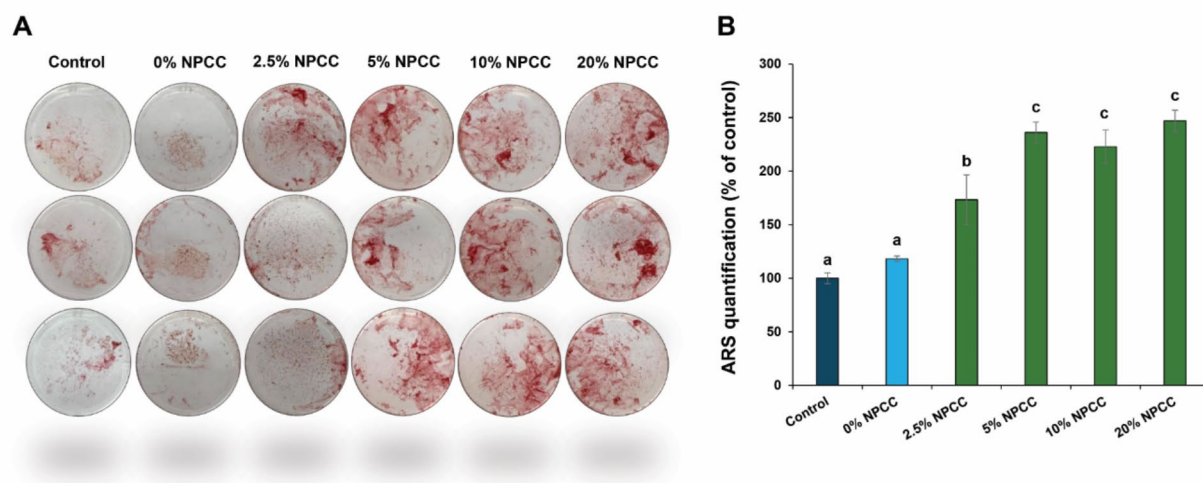

Fig. 4. In vitro mineralization of BMSC cultures exposed to CSC-NPCC eluent for 30 d. (A) Representative images of alizarin red S-stain (ARS) mineral deposits. (B) Quantitative analysis of ARS staining from three independent experiments ($n = 3$). Data bars labeled with different letters indicate statistically significant differences among the groups ($P < 0.05$).

cross-sectional images of the implantation sites at two months post-implantation. As shown in Fig. 5A, in the femurs implanted with CSC alone, a substantial portion of the cement remained intact over the two-month period. CSC occupied 22.2%±3.25% of the total area of the femur. Newly formed bone was observed along the boundaries of the CSC cement. CSC-NPCC (5%) persisted in the femur to a similar extent as CSC alone. However, unlike CSC alone, CSC-NPCC (10%) and CSC-NPCC (20%) underwent significant resorption, with the cement occupying only 4% of the femoral area in the CSC-NPCC (20%) group (Fig. 5C). In the region between the cement and the bone, areas appeared where the cement and tissue were intermingled. Masson's trichrome-stained images suggested the coexistence of cement and connective tissues in areas where cement was presumed to be undergoing resorption and replacement by bone (Fig. 5B). The area of the newly formed bone increased proportionally with the concentration of NPCC (Fig. 5D). The histological results suggested that NPCC facilitates CSC resorption, followed by bone regeneration in the resorbed area.

Discussion

NPCC was introduced in industrial engineering to accelerate the setting of concrete[20]. Other previous studies have explained that the effect of NPCC on setting time is likely due to an increase in contact points as a nucleation site[14,15,20]. Thus, it was anticipated that NPCC would be more effective in accelerating the setting process compared to microsized particles owing to their numerous nucleation sites. However, a similar accelerating effect on setting time has also been observed with microsized calcium carbonate particles[17,21,22], suggesting that the particle size may not be a critical factor in modulating the setting time. Further investigation of calcium carbonate particles across a range of sizes is needed to better understand the influence of particle size on the setting behavior of calcium silicate cements.

As indicated by the data (Table 1), NPCC caused a significant reduction in the compressive strength of CSC at higher concentrations, which is consistent with previous reports using MTA and NPCC[15]. In contrast to NPCC, microsized calcium carbonate particles have been demonstrated to increase the compressive strength of
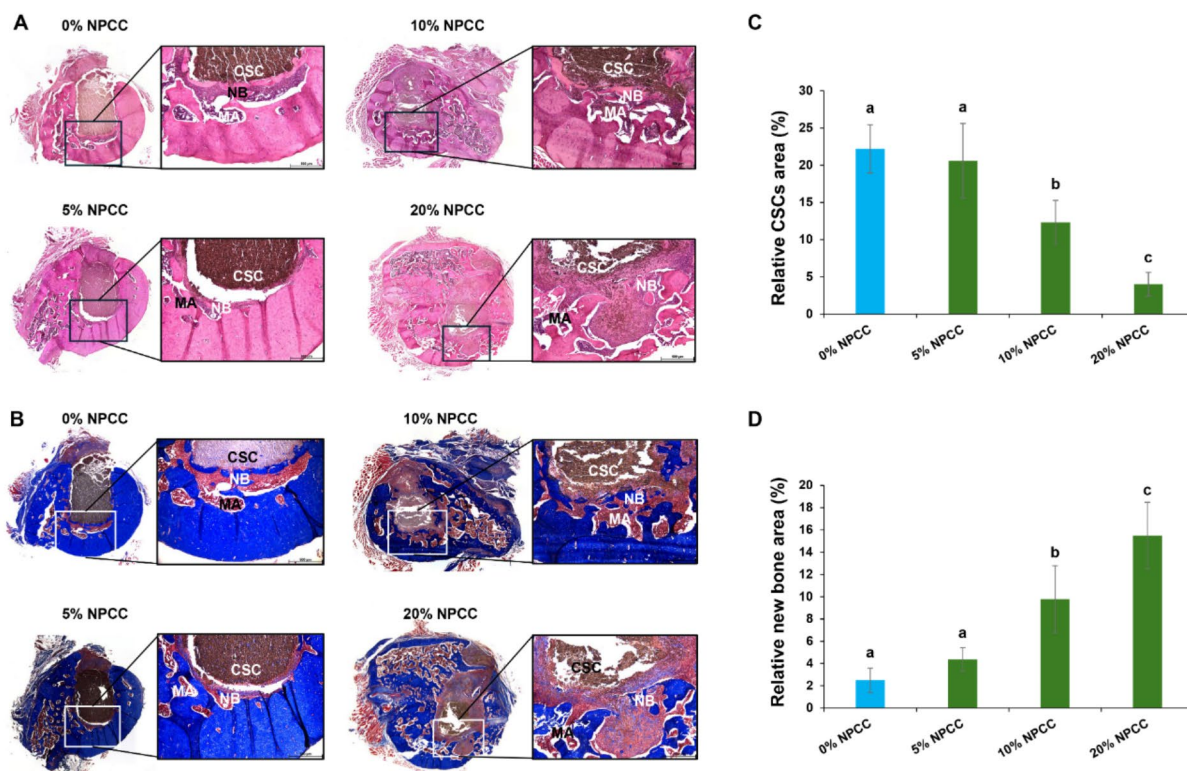
Fig. 5. Interaction between CSC-NPCC and rat femur tissue. (A) H&E staining images showing the presence of CSC, bone marrow (MA), and new bone (NB). (B) Masson's trichrome staining of CSC-NPCC-implanted femur tissue. (C) Relative area of CSCs as a percentage of the total femoral area. (D) Relative area of new bone as a percentage of the total femoral area. Data bars with different letters indicate statistically significant differences among the groups ($P < 0.05$).

tricalcium silicate cement[21,23]. These differences in the influence of calcium carbonate on compressive strength may be attributed to various factors, including the size of the calcium carbonate particles, water-to-powder ratio, the composition of the cements, and other related variables. NPCC decreased the solubility of CSC at all the tested concentrations, except at 5%. This observed decrease in solubility contrasts with previous studies, which demonstrated that calcium carbonate particles at both the nano- and micro-sized scales increased the solubility of MTA and CSC[15,21,24]. Although the underlying reason for this inconsistency is not understood, it is hypothesized that alterations in the composition of CSC may influence the effect of calcium carbonate on cement solubility.

The incorporation of NPCC into CSC promoted the osteogenic differentiation of BMSCs. This effect was likely due to the increased release of calcium ions resulting from the dissolution of calcium carbonate. Alternatively, NPCC may enhance calcium ion release directly from CSC. The enhanced osteogenic activity of CSCs induced by NPCC suggests the potential utility of CSC-NPCC for bone regeneration in bone defects. Unset cement was implanted in rat femurs to assess the effects of CSC-NPCC on bone defects. As shown in Fig. 5, the interactions between CSC and the surrounding tissues varied depending on the concentration of NPCC within the CSC. In the femurs filled with CSC alone, the cement was distinguishable from the surrounding tissue, suggesting minimal resorption. A quantitative analysis of the CSC area in the femurs demonstrated that cement resorption became more pronounced with increasing NPCC concentration. In contrast to untreated CSC, CSC with high concentrations of NPCC formed areas containing a mixture of bone and particulate cement. It is hypothesized that the mixed area represents a transitional zone in which cement resorption and new bone formation occur simultaneously. As there was no void zone surrounding the cement, the velocity of cement resorption likely did not exceed that of bone formation. The promotion of osteogenic differentiation by CSC with NPCC is likely associated with its bone-forming capacity. The higher degree of resorption observed in CSC-NPCC may be attributed to the dissolution of calcium carbonate, which enhances the interaction between the cement and bone marrow.

Abd-Elkawi et al. demonstrated the effect of NPCC on new bone formation in a rabbit bone defect model[25]. In this study, NPCC alone was less effective in promoting bone formation but exhibited greater efficacy when combined with silver nanoparticles and platelet-rich fibrin, suggesting that NPCC may need to be combined with other additives to optimize its function in bone formation. In our study, the combination of CSC and NPCC demonstrated the ability to promote new bone formation, accompanied by cement resorption. Given the bonding properties of CSC, CSC-NPCC can be regarded as a bone cement with the potential to facilitate bone regeneration. CSCs are also recognized for their antimicrobial properties, which can be attributed to the elevated pH generated during hydration[26,27]. This suggests the potential utility of CSC-NPCCs for bone regeneration in infected bone defects.

In conclusion, NPCCs enhanced the osteogenic activity and increased the biodegradability of CSC, making CSC-NPCC a suitable bone cement for use in bone defect areas requiring regeneration.

Materials and methods
Preparation of CSC and CSC-NPCC mixture
CSC were prepared as described previously[28]. In brief, calcium carbonate (Daejung, Seoul, Korea), silicon dioxide (SiO_2, Junsei, Tokyo, Japan), and aluminum oxide (Al_2O_3, Junsei) were mixed, to which DW was added, followed by drying at 100 °C for 1 d. The mixture was precalcined at 800–900 °C and annealed at 1300–1450 °C. The calcined particles were then ground with zirconium balls and sieved using a vibratory sieve shaker (AS 200; Retsch, Düsseldorf, Germany). Finally, the CSC was blended with NPCC (US Research Nanomaterials, Houston, Texas, USA) at varying concentrations ranging from 2.5 to 20% by weight. The morphologies of CSC and NPCC were observed using SEM (Apreo S, Thermo Fisher Scientific, Waltham, MA, USA), and the chemical compositions were analyzed using XRD (D8 ADVANCE, Bruker, Karlsruhe, Germany) with Cu-Kα radiation (40 kV and 40 mA).

Analysis of physicomechanical properties of CSC-NPCC
The setting time of CSC-NPCC was determined according to ISO 6876/2012[29]. The cement was mixed with DW at a ratio of 1:0.8 and filled into a metal-ring mold (10 mm in diameter and 2 mm in height). A Gillmore needle, with a mass of 100 g and a cylindrical tip of 2 mm in diameter, was applied to the surface of the cement. The sample was maintained at 37 °C and 95% humidity between tests. The solubility was measured according to ISO 6876/2012[29]. After mixing with DW, CSC-NPCC specimens (20 mm in diameter, 1.5 mm in height) were stored at 37 °C under 95% humidity for 1 d. The specimens were then carefully cleaned of excess cement using 600-grit sandpaper (Deerfos, Seoul, Korea) and weighed using a precision analytical balance (Adventurer AR2140; Ohaus Corp., Parsippany, New Jersey, USA). The two hydrated cement samples were placed in a glass dish containing 50 mL of DW and incubated at 37 °C for 24 h. After the 24 h soaking period, the samples were removed, washed with 3 mL DW and the dissolved substance was quantified by evaporating the DW at 110 ± 2 °C. The solubility of the cement was determined by calculating the percentage difference in mass between the initial and final weights of the dish. The compressive strength was measured according to ISO 9917-1/2007[30]. CSC-NPCC was mixed with DW and placed in a cylindrical stainless-steel mold (5 mm in diameter, 8 mm in height). After it was cured for 1 d at 37 °C under 95% humidity, the compressive strength was determined using an Instron 8871 (Norwood, MA, USA) at a crosshead speed of 0.75 mm/min. The compressive strength was calculated in megapascals (MPa) according to the following formula:

$$C = \frac{4P}{\pi D^2}$$

Gene	Forward	Reverse
GAPDH	TGTGTCCGTCGTGGATCTGA	CCTGCTTCACCACCTTCTTGAT
RUNX2	CCACCACTCACTACCACACG	TATGGAGTGCTGCTGGTCTG
ALP	CACAGATTCCCAAAGCACCT	GGGATGGAGGAGAGAAGGTC
COL-1	ACTGGTACATCAGCCCGAAC	AATCCATCGGTCATGCTCTC
OCN	GCGCTCTGTCTCTCTGACCT	ACCTTATTGCCCTCCTGCTT

Table 2. RT-qPCR primers.

Where P represents the maximum load recorded by the machine in newtons (N) and D is the diameter of the sample in millimeters (mm), and C is the compressive strength in MPa. Dimensional stability was measured according to ISO 6876/2001[31]. The cement was mixed and placed into a split metal mold (6 mm in diameter, 12 mm in height). Once set, the samples were stored in an incubator at 37 °C with 95% humidity. After 24 h, the surface of each sample was polished with 600-grit sandpaper (Deerfos). The initial length of the sample was recorded using a digital calliper (Mitutoyo, Tokyo, Japan). The sample was then dipped in a separate container containing 20 mL of DW and maintained at 37 °C for 30 d. After this period, the length was measured again.

The dimensional change was calculated using the following formula:

$$Dimensional\ change\ (\%) = \frac{L_{final} - L_{initial}}{L_{initial}} \times 100$$

Isolation of mouse BMSCs
BMSCs were isolated from mouse femurs following approval from the Institutional Animal Care and Use Committee (IACUC) of Seoul National University (SNU-240220-3). Five-week-old ICR mice (Orient Bio Inc., Seongnam, Korea) were humanely sacrificed, and bone marrow femurs were extracted by flushing with phosphate-buffered saline (pH = 7.4) using a syringe. The extracts were centrifuged at 1,500 rpm for 5 min, and the pellet was resuspended in minimum essential medium alpha modification (Alpha MEM; Welgene, Gyeongsan, Korea) supplemented with 10% fetal bovine serum (FBS) (Welgene) and 1% penicillin/streptomycin (Welgene). The cell suspension was subsequently cultured for one week, with the medium changed every other day to remove nonadherent cells. Finally, the cells were subcultured until the third passage for in vitro experiments.

Cytotoxicity assessment
The cytotoxicity of CSC-NPCC was assessed by treating the BMSCs with hydrated CSC-NPCC eluents. To prepare the eluents, the CSC-NPCC powder was mixed with DW, set for 24 h, and sterilized under UV light for 20 min. The specimen was then soaked in Dulbecco's modified Eagle medium (DMEM) (Welgene) containing 10% FBS and 1% antibiotics for 72 h at 37 °C. The eluents were filtered through 0.2 μm pore-size syringe filters (Minisart HF, Sartorius, Gottingen, Germany), and subjected to serial dilutions with culture media. For the treatment of the cells, the BMSCs were seeded in a 96-well plate (0.8×10^4 cells/well), incubated at 37 °C for 24 h in a humidified atmosphere of 5% CO_2, and treated with the culture media containing the CSC-NPCC eluents. The viability of the treated cells was determined using a WST assay kit (DoGenBio, Seoul, Korea). Briefly, 10 μL EZ-Cytox of the assay kit was added to each well for a reaction for 1 h, and the absorbance was measured at 450 nm using a microplate reader (INNO, LTEK, Seongnam, Korea).

Osteogenic activity assay
The effect of CSC-NPCC on the expression of the osteoblast marker genes and the mineralization activity of the BMSCs was observed. The BMSCs were cultured in DMEM containing 25% CSC-NPCC eluent and osteogenic-differentiation-inducing factors (OIFs), which included 50 μM ascorbic acid, 10 mM β-glycerophosphate, and 10 nM dexamethasone. After 10 d of treatment, the mRNA expression levels of RUNX2, ALP, COL-1, and OCN were evaluated using quantitative reverse transcription polymerase chain reaction (RT-qPCR). An RNA isolation reagent (WellPrep Total RNA Isolation Reagent, Welgene) and a cDNA synthesis kit (Power cDNA Synthesis Kit, iNtRON Biotechnology, Sungnam, Korea) were used to isolate the total RNA and synthesize cDNA, respectively. PCR was performed using the SYBR Premix Ex and ROX Reference Dye (Takara Bio, Otsu, Japan). The mRNA level of glyceraldehyde-3-phosphate dehydrogenase (GAPDH) was used as an expression control. The primer sequences used in this study are listed in Table 2.

The effect of CSC-NPCC on the mineralization of the BMSC extracellular matrix was explored using an alizarin red S (ARS) staining assay. The BMSCs were cultured in DMEM containing a 25% eluent of cement and OIFs for 30 d, with the medium changed every 2 d. The cultures were then fixed with 4% paraformaldehyde for 15 min, stained with 40 mM ARS solution (pH 4.3) for 30 min, and washed with DW. Images were obtained to visualize the calcium deposition, and the amount of ARS was quantified as described previously[28].

Implantation of CSC-NPCC into rat femurs
CSC-NPCC was implanted in accordance with the guidelines of the IACUC of Seoul National University (SNU-240220-3). Male Sprague Dawley rats (Orient Bio Inc.) (8 weeks old, weighing 250–300 g) were anesthetized by an intraperitoneal injection of ketamine (Yuhan Co., Kunpo, Korea) and xylazine (Rompun, Bayer HealthCare, Leverkusen, Germany) at a ratio of 4:1 (v/v). Twelve rats were randomly allocated to four groups (three rats per group): one CSC (0% NPCC) group and three CSC-NPCC (5%, 10%, and 20% NPCC) groups (each group

included 3 rats with 6 femoral holes). For implantation, a circular cylindrical defect (2 mm in diameter and 4 mm in depth) was created in the proximal portion of femoral shaft through a minimal incision, after which the test cement was used to fill the defect, and the incision was sutured. After eight weeks, the rats were sacrificed using CO_2 hyperventilation. The rat femurs were separated, formalin-fixed, and decalcified in 10% formic acid at 4 °C for 2 d. Then, the specimens were embedded in paraffin blocks, sectioned at a thickness of 5 μm, and stained with H&E (BBC Biochemical, Mount Vernon, WA, USA) and Masson's trichrome (ScyTek, Logan, Utah, USA). Images of the stained sections were captured using an upright microscope (DM6B; Leica, Wetzlar, Germany) equipped with a digital camera (DFC7000T; Leica). The ImageJ software (Bethesda, MD, USA) was used to measure the area occupied by CSC and new bone in the stained images.

Statistical analysis

All the data are presented as the mean ± standard deviation. One-way analysis of variance (ANOVA) was used for the statistical analysis of all experiments, except for the cytotoxicity assay, which was analyzed using a Student's t-test. SPSS (version 25.0; IBM, Armonk, NY, USA) was used to analyze the data, with ANOVA followed by Tukey's post-hoc test. Statistical significance was set at $P < 0.05$.

Data availability

The datasets generated and/or analyzed in the current study are available from the corresponding author upon-reasonable request.

References

1. Nair, P. N., Duncan, H. F., Ford, P., Luder, H. U. & T. R. & Histological, ultrastructural and quantitative investigations on the response of healthy human pulps to experimental capping with mineral trioxide aggregate: a randomized controlled trial. *Int. Endod J.* **41**, 128–150 (2008).
2. Felippe, W. T., Felippe, M. C. & Rocha, M. J. The effect of mineral trioxide aggregate on the apexification and periapical healing of teeth with incomplete root formation. *Int. Endod J.* **39**, 2–9 (2006).
3. Apaydin, E. S., Shabahang, S. & Torabinejad, M. Hard-tissue healing after application of fresh or set MTA as root-end-filling material. *J. Endod.* **30**, 21–24 (2004).
4. Camilleri, J. Mineral trioxide aggregate: present and future developments. *Endod Top.* **32**, 31–46 (2015).
5. Farrugia, C., Baca, P., Camilleri, J. & Moliz, M. T. A. Antimicrobial activity of ProRoot MTA in contact with blood. *Sci. Rep.* **7**, 41359 (2017).
6. Dammaschke, T., Nowicka, A., Lipski, M. & Ricucci, D. Histological evaluation of hard tissue formation after direct pulp capping with a fast-setting mineral trioxide aggregate (RetroMTA) in humans. *Clin. Oral Investig.* **23**, 4289–4299 (2019).
7. Gomes-Cornélio, A. L. et al. Bioactivity of MTA plus, Biodentine and an experimental calcium silicate-based cement on human osteoblast-like cells. *Int. Endod J.* **50**, 39–47 (2017).
8. Margunato, S., Taşlı, P. N., Aydın, S., Karapınar Kazandağ, M. & Şahin, F. In vitro evaluation of ProRoot MTA, Biodentine, and MM-MTA on human alveolar bone marrow stem cells in terms of biocompatibility and mineralization. *J. Endod.* **41**, 1646–1652 (2015).
9. Torabinejad, M., Hong, C. U., McDonald, F. & Pitt Ford, T. R. Physical and chemical properties of a new root-end filling material. *J. Endod.* **21**, 349–353 (1995).
10. Lee, B. N. et al. Improvement of the properties of mineral trioxide aggregate by mixing with hydration accelerators. *J. Endod.* **37**, 1433–1436 (2011).
11. Huang, T. H., Shie, M. Y., Kao, C. T. & Ding, S. J. The effect of setting accelerator on properties of mineral trioxide aggregate. *J. Endod.* **34**, 590–593 (2008).
12. Bortoluzzi, E. A. et al. The influence of calcium chloride on the setting time, solubility, disintegration, and pH of mineral trioxide aggregate and white Portland cement with a radiopacifier. *J. Endod.* **35**, 550–554 (2009).
13. Kakali, G., Tsivilis, S., Aggeli, E. & Bati, M. Hydration products of C3A, C3S and Portland cement in the presence of $CaCO_3$. *Cem. Concr Res.* **30**, 1073–1077 (2000).
14. Sato, T. & Diallo, F. Seeding effect of nano-$CaCO_3$ on the hydration of tricalcium silicate. *Transp. Res. Rec.* **2141**, 61–67 (2010).
15. Bernardi, A. et al. Effects of the addition of nanoparticulate calcium carbonate on setting time, dimensional change, compressive strength, solubility and pH of MTA. *Int. Endod J.* **50**, 97–105 (2017).
16. Khalil, I., Naaman, A. & Camilleri, J. Investigation of a novel mechanically mixed mineral trioxide aggregate (MM-MTA). *Int. Endod J.* **48**, 757–767 (2015).
17. Köseoglu, S. et al. Biological response of commercially available different tricalcium silicate-based cements and pozzolan cement. *Microsc Res. Tech.* **80**, 994–999 (2017).
18. Bortoluzzi, E. A. et al. Cytotoxicity and osteogenic potential of silicate calcium cements as potential protective materials for pulpal revascularization. *Dent. Mater.* **31**, 1510–1522 (2015).
19. Esen, M., Guven, Y., Seyhan, M. F., Ersev, H. & Tuna-Ince, E. B. Evaluation of the genotoxicity, cytotoxicity, and bioactivity of calcium silicate-based cements. *BMC Oral Health.* **24**, 119 (2024).
20. Camiletti, J., Soliman, A. M. & Nehdi, M. L. Effect of nano-calcium carbonate on early-age properties of ultra-high-performance concrete. *Mag Concr Res.* **65**, 297–307 (2013).
21. Huan, Z. G. & Chang, J. Study on physicochemical properties and in vitro bioactivity of tricalcium silicate-calcium carbonate composite bone cement. *J. Mater. Sci. Mater. Med.* **19**, 2913–2918 (2008).
22. Camilleri, J., Sorrentino, F. & Damidot, D. Investigation of the hydration and bioactivity of radiopacified tricalcium silicate cement, Biodentine and MTA angelus. *Dent. Mater.* **29**, 580–593 (2013).
23. Wang, X. et al. Effect of biological shells aggregate on the mechanical properties and sustainability of concrete. *Sci. Rep.* **14**, 10615 (2024).
24. Prati, C. & Gandolfi, M. G. Calcium silicate bioactive cements: biological perspectives and clinical applications. *Dent. Mater.* **31**, 351–370 (2015).
25. Abd-Elkawi, M., Sharshar, A., Misk, T., Elgohary, I. & Gadallah, S. Effect of calcium carbonate nanoparticles, silver nanoparticles and advanced platelet-rich fibrin for enhancing bone healing in a rabbit model. *Sci. Rep.* **13**, 15232 (2023).
26. Jang, Y. J. et al. Physicochemical, biological, and antibacterial properties of four bioactive calcium silicate-based cements. *Pharmaceutics* **15**, 1701 (2023).

27. Huang, S. C., Wu, B. C. & Ding, S. J. Stem cell differentiation-induced calcium silicate cement with bacteriostatic activity. *J. Mater. Chem. B*. **3**, 570–580 (2015).
28. Son, G., Seon, G. M., Choi, S. H. & Yang, H. C. Effects of vehicles on the physical properties and biocompatibility of premixed calcium silicate cements. *Dent. Mater. J.* **43**, 276–285 (2024).
29. International Organization for Standardization. *Dentistry: Dental Root Canal Sealing Materials*, (2012).ISO (6876).
30. International Organization for Standardization. ISO 9917-1. Dentistry. Water-Based Cements: Part 1,. (2007).
31. International Organization for Standardization. *Dentistry: Dental Root Canal Sealing Materials*, (2001).ISO (6876).

Acknowledgements

Author contributions

Q.C.V. and G.S conducted the experiments, histological processing, data collection, statistical analysis and wrote original draft. G.M.S., S.W.U., and S.H.C. contributed to the development of methodology and data analysis. H.C.Y. designed conception and research, performed supervision and writing – review & editing the manuscript. All authors read and approved the final manuscript.

Declarations

Competing interests

The authors declare no competing interests.

Ethical approval

This study was approved by the Institutional Animal Care and Use Committee (IACUC) of Seoul National University (SNU-240220-3). All the ethical standards for animal research were followed and implemented in accordance with international and institutional guidelines, particularly the ARRIVE guidelines.

Additional information

Correspondence and requests for materials should be addressed to H.-C.Y.

Reprints and permissions information is available at www.nature.com/reprints.

Publisher's note Springer Nature remains neutral with regard to jurisdictional claims in published maps and institutional affiliations.